Spatiotemporal Modelling of Multi-Gateway LoRa Networks with Imperfect SF Orthogonality

Bouazizi, Y., Benkhelifa, F. & McCann, J.

Original citation & hyperlink:
Bouazizi, Y, Benkhelifa, F & McCann, J 2021, Spatiotemporal Modelling of Multi-Gateway LoRa Networks with Imperfect SF Orthogonality. in 2020 IEEE Global Communications Conference, GLOBECOM 2020 - Proceedings. IEEE, 2020 IEEE Global Communications Conference, Taipei, Taiwan, Province of China, 7/12/20. https://dx.doi.org/10.1109/GLOBECOM42002.2020.9322640

DOI 10.1109/GLOBECOM42002.2020.9322640
ISBN 9781728182995
ISBN 9781728182988

Publisher: IEEE

Spatiotemporal Modelling of Multi-Gateway LoRa Networks with Imperfect SF Orthogonality

Yathreb Bouazizi, Fatma Benkhelifa, Julie McCann
Imperial College London, London, UK
{y.bouazizi18,f.benkhelifa,j.mccann}@imperial.ac.uk

***Abstract*—Meticulous modelling and performance analysis of Low-Power Wide-Area (LPWA) networks are essential for large scale dense Internet-of-Things (IoT) deployments. As Long Range (LoRa) is currently one of the most prominent LPWA technologies, we propose in this paper a stochastic-geometry-based framework to analyse the uplink transmission performance of a multi-gateway LoRa network modelled by a Matern Cluster Process (MCP). The proposed model is first to consider all together the multi-cell topology, imperfect spreading factor (SF) orthogonality, random start times, and geometric data arrival rates. Accounting for all of these factors, we initially develop the SF-dependent collision overlap time function for any start time distribution. Then, we analyse the Laplace transforms of intra-cluster and inter-cluster interference, and formulate the uplink transmission success probability. Through simulation results, we highlight the vulnerability of each SF to interference, illustrate the impact of parameters such as the network density, and the power allocation scheme on the network performance. Uniquely, our results shed light on when it is better to activate adaptive power mechanisms, as we show that an SF-based power allocation that approximates LoRa ADR, negatively impact nodes near the cluster head. Moreover, we show that the interfering SFs degrading the performance the most depends on the decoding threshold range and the power allocation scheme.**

***Index Terms*—LoRa, Stochastic Geometry, imperfect SF orthogonality, random start time, collision time overlap, success probability.**

I. Introduction

Low-Power Wide-Area (LPWA) Networks (LPWANs) are emerging as a prominent communication solution, addressing the challenging growth, ubiquity, and diversity of the Internet-of-Things (IoT) landscape, while reconciling low-cost and low-energy requirements. LoRa is currently one of the promising solutions among emerging LPWA technologies. LoRa accommodates several tune-able technical parameters like the spreading factor (SF), which specifies the number of bits per symbol, the coding rate (CR), which determines the number of bits used for error correction, transmit power and bandwidth (Bw) [1]. By tuning these parameters, LoRa offers adaptive schemes that can answer different IoT scenarios and applications requirements. It is important to understand how such parameters affect performance.

Indeed several studies have looked into LoRa performance analysis and optimisation [2]–[11]. However, most of these studies assume perfect SF-orthogonality and almost exclusively limit their investigations to the impact of interference coming from the nodes using the same SF. From this perspective, a LoRa network can be interpreted as the aggregation of independent sub-networks, each operating in a different SF. Under the aforementioned assumption, the performance of a multi-cell LoRa network coexisting with other unlicensed radio technologies was studied in [2]. In [3], the scalability analysis of a single LoRa cell was provided. However, the outage condition was formulated based only on the dominant interfering signal.

The assumption of perfect orthogonality has been empirically questioned in [4]. Few research studies have, hence, begun to consider non-perfect or quasi-orthogonality use cases. Among these studies, some works explored geometry-less schemes like [5], [6], while other works used a geometry-based approach like [7], which modelled a multi-cell LoRa network using two different cluster processes: Matern Cluster Process and Matern Hard core Process. Besides, in their signal-to-interference and noise ratio (SINR) formulations, most of the works considered co-subchannel rejection thresholds between each two SFs by considering the interference from only one SF-set [5], [7], [8]. The first concern regarding such thresholds is that they are empirical and hence not unique. For instance, the values empirically validated in [4] and adopted in [7] are different from those in [10] which are used in [8]. The second concern about this approach is whether or not it captures correct decoding methods at the gateway level. Does a LoRa gateway decode the signal using a pairwise-scheme based on the SF value of the interfering packet? For these reasons, we choose to conduct the analysis following a more general approach by varying the range of decoding thresholds and considering interference from all the SFs.

The absence of coordination between nodes in LoRa Aloha-like asynchronous system leads to an interfering power that changes over time. Although essential, especially with the SF-related variable packet's time on-air (ToA), interference time dependence has been generally underestimated and neglected in LoRa network analysis. Only a few studies have integrated it, such as [8] [9]. In [8] a collision time probability distribution was formulated based on the difference between uniform

This work is supported by the Singapore Ministry of National Development and the National Research Foundation, Prime Minister's Office under the Land and Liveability National Innovation Challenge (L2NIC) Research Programme (L2 NIC Award No. L2NICTDF1-2017-3). Any opinions, findings, and conclusions or recommendations expressed in this material are those of the author(s) and do not reflect the views of the Singapore Ministry of National Development and National Research Foundation, Prime Minister's Office, Singapore.

start times and used to analyse SF allocation in a single gateway topology assuming the rejection thresholds previously mentioned. In [9], a spatiotemporal density was used to study a single gateway under only co-SF interference which resulted in treating LoRa like pure Aloha.

In this paper, we aim to bridge these research gaps by considering the analysis of LoRa uplink transmissions in a multi-cell topology with imperfect orthogonality between different SFs and random transmission start times. We use stochastic geometry, which is known for its ability to capture different sources of randomness within the network [12]. Our main contributions are summarized as follows:

- A Novel spatiotemporal mathematical model is presented for a multi-gateway LoRa network; it accounts for the imperfect SF-orthogonality and the collision overlap time.
- The SF-based collision overlap time function is formulated for random transmission start times.
- A general analytical expression of the transmission success probability is derived; it can scale down to particular cases and other published works.
- The vulnerability of SFs to interference is assessed, and their relationship to one another performance is analyzed.
- The network parameters that impact the success transmission probability, and hence the scalability of the network are studied, including node density, power allocation schemes, and decoding thresholds.

II. System Model

In this paper, we use a Matern Cluster Process (MCP) to model a multi-gateway LoRa network. This cluster process allows us to account for the clustered-nature of LoRa, as an operator-free potentially unplanned technology. According to this cluster process, LoRa gateways L_i are distributed following a homogeneous Poisson Point Process (PPP) $\Phi_G = \{y_i, i = 1,2,\dots\}$ with intensity λ_G, where $y_i \in \mathbb{R}^2$ is the location of the i'th LoRa gateway. Each cluster C_i centred is at L_i and has a radius R. Within the area of each cluster, LoRa end-devices (EDs) are uniformly scattered around L_i and form a PPP $\Phi_{ED,i} = \{x_{ij}, j = 1,2,\dots\}$ of intensity λ_{ED}, where $x_{ij} \in \mathbb{R}^2$ is the location of the j'th LoRa ED in the i'th cluster. The overall superposition of $\Phi_{ED,i}$ captures the position of all the children nodes and gives the desired MCP-based network.

Furthermore, each LoRa ED can be assigned to an SF in $\mathcal{S}$={$\mathbf{SF_1},\dots,\mathbf{SF_N}$} , where N is the total number of available SFs. We adopt an equal-interval-based (EIB) SF allocation scheme for which each cluster C_i is divided into N annuli A_q delimited by d_{q-1} and d_q, where $q \in Q$={ $\mathbf{1},\mathbf{2},...,\mathbf{N}$} is standing for the q'th SF. Each annulus A_q is of width $\omega = \frac{R}{N}$ and hence $d_{q-1} = (q-1)\omega$ and $d_q = q\omega$. The average nodes number in each annulus is $N_q = \lambda_{ED}\pi(d_q^2 - d_{q-1}^2)$.

The overall spatio-temporal model of the network can be interpreted as an independently marked process where the ground process is formed by the nodes positions and the marks represent the transmission start time of each node [13]. The time marks are independent since the medium access technique used by LoRa is un-slotted Aloha-like where nodes send their packets independently without any prior coordination or synchronization. At each device, the packets are generated according to a geometric distribution with parameter $a \in [0,1]$. By virtue of the independent thinning of a homogeneous PPP [14], the subset of transmitting nodes form a homogeneous PPP $\tilde{\Phi}_{ED,i}$ of intensity aλ_{ED} (See Fig.1). We consider a power-law path-loss propagation model where the signal attenuates with the propagation distance at the rate $r^{-\eta}$, $\eta > 2$ is the path-loss exponent. Added to the large scale fading, we have Rayleigh block fading channels with unit mean exponentially distributed channel gains g_{ij}, i.e. $g_{ij} \sim exp(1)$. All the channels are assumed to be independent of the space and time dimensions.

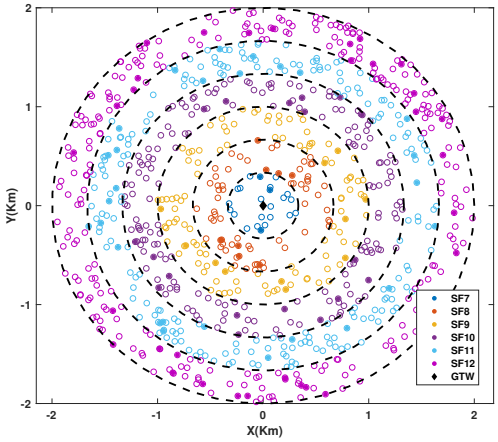

Figure 1: Example of EIB SF allocation in a single-gateway LoRa network with active (filled dots) and inactive (empty dots) nodes, with $a = 0.1$, $\lambda_{ED} = 80$ nodes/Km^2, and $R = 2$ Km.

III. Stochastic Geometry Analysis

The received Signal to Interference and Noise Ratio (SINR) at the typical LoRa receiver from a typical LoRa node, located at $r_0 = \|x_{00}\|$ and emitting with SF $q_0 \in Q$, is formulated as:

$$SINR(r_0, q_0) = \frac{P_t g_{00} \alpha r_0^{-\eta}}{I_{intra} + I_{inter} + \sigma^2}, \quad (1)$$

where I_{intra} is the intra-cluster interference coming from active nodes within the same cluster, I_{inter} is the inter-cluster interference originating from transmitting nodes in other clusters, and σ^2 is the variance of the additive white Gaussian noise (AWGN). I_{intra} and I_{inter} account for interference from the same SF (Co-SF) and from different SFs (Inter-SF).

A. SF-Dependent Collision Overlap Time

As LoRa uses interleaving and repetition codes, we consider an averaging over the exchanged packet duration to account for the time dependence of the interference [13]. In contrast to ordinary Aloha models, LoRa has a variable packet duration l_q since the packet Time-On-Air (ToA) is linked to the SF

used in the transmission. The variable time-on-air leads to an SF-dependent collision overlap time.

We consider a typical LoRa node located at $x_{00} \in \tilde{\Phi}_{ED,0}$ emitting with SF $q_0 \in Q$ and communicating with a typical gateway placed at the origin. Without loss of generality, we assume that the typical LoRa node starts its desired transmission with $SF = q_0$ at $T_0 = 0$. The time-averaged I_{intra} and I_{inter} interference experienced by the receiver are given by:

$$I_{intra} = I_{intra}^{mean} = \frac{1}{l_{q_0}} \int_{T_0}^{T_0+l_{q_0}} I_{intra}(t)dt = \sum_{q\in Q} \sum_{x\in\tilde{\Phi}_{ED,0}\setminus x_{00}} \mathbb{1}_{j,q} P_q \alpha \|x_{0j}\|^{-\eta} h_{q_0,q}(T_{ij}) g_{0j}, \quad (2)$$

$$I_{inter} = I_{inter}^{mean} = \frac{1}{l_{q_0}} \int_{T_0}^{T_0+l_{q_0}} I_{inter}(t))dt = \sum_{q\in Q} \sum_{y\in\Phi_G\setminus y_0} \sum_{x\in\ \tilde{\Phi}_{ED,i}} \mathbb{1}_{j,q} P_q \alpha \|y_i + x_{ij}\|^{-\eta} h_{q_0,q}(T_{ij}) g_{ij}, \quad (3)$$

where $\mathbb{1}_{j,q}$ is the indicator function of ED_j transmitting at SF q and $h_{q_0,q}(T_{ij})$ is the collision overlap time function between the LoRa node located at $x_{ij} \in \tilde{\Phi}_{ED,i}$ with random transmission start time T_{ij} and the typical user. $h_{q_0,q}(T_{ij})$ is expressed as:

$$h_{q_0,q}(T_{ij}) = \frac{1}{l_{q_0}} \int_{T_0}^{T_0+l_{q_0}} \mathbb{1}(\ x_{ij} \text{ overlaps with } x_{00}) \quad d(t), \quad (4)$$

Because of duty cycle restriction where a node is active only for %1 and since $l_6 < 100 \times l_1$, a desired packet will not be interfering with a first and second transmissions from the same node. Assuming all the active nodes (except the typical user) start transmitting randomly in a contention window $[-T_c, T_c]$. The collision overlap time is expressed in the following lemma:

Lemma 1. *The collision overlap time function $h_{q_0,q}(T_{ij})$ between the desired node x_{00} and the interfering node x_{ij} transmitting with SF q at random time T_{ij} is*

$$h_{q_0,q}(T_{ij}) = \begin{cases} \frac{l_{q_0}-T_{ij}}{l_{q_0}}, & if\ \left(l_{q_0}-l_q\right)^+ \le T_{ij} \le l_{q_0}, \\ \frac{\min\left(l_{q_0},l_q\right)}{l_{q_0}}, & if\ -\left(l_q-l_{q_0}\right)^+ \le T_{ij} \le \left(l_{q_0}-l_q\right)^+, \\ \frac{l_q+T_{ij}}{l_{q0}}, & if\ -l_q \le T_{ij} \le -\left(l_q-l_{q_0}\right)^+, \\ 0, & if\ -T_c \le T_{ij} < -l_q\ or\ l_{q_0} < T_{ij} \le T_c, \end{cases} \quad (5)$$

where $(t)^+ = max(t, 0)$.

Proof. The proof is in Appendix A. □

Corollary 1. *Using Lemma 1, and assuming that the transmission starting time of the interfering nodes is uniformly distributed between $[-T_c, T_c]$, $T_{ij} \overset{Dist}{=} U(-T_c, T_c)$, we show that*

$$\mathbb{E}_{T_{ij}}\left[\frac{1}{1+uh_{q0,q}\left(T_{ij}\right)}\right] = 1 - \frac{l_{q_0}+l_q}{2T_c} + \frac{l_{q_0}}{T_c u}\log\left(u\frac{min\left(l_q,l_{q_0}\right)}{l_{q_0}}+1\right) + \frac{\left|l_{q_0}-l_q\right|}{2T_c\left(1+u\frac{min\left(l_q,l_{q_0}\right)}{l_{q_0}}\right)}, \quad (6)$$

where $\mathbb{E}_{T_{ij}}[\cdot]$ is the expectation operator with respect to T_{ij}.

Proof. The proof is in Appendix B. □

B. Transmission Success Probability

The typical LoRa gateway is able to receive and successfully decode the desired signal if its instantaneous SINR surpasses a reference decoding threshold γ_{th} as

$$\begin{aligned} P_{Succ}(r_0, q_0) &= P\{SINR(r_0, q_0) \ge \gamma_{th}\} \\ &\overset{(a)}{=} e^{-\rho\sigma^2}\mathbb{E}_{I_{intra}}\{e^{-\rho I_{intra}}\}\mathbb{E}_{I_{inter}}\{e^{-\rho I_{inter}}\} \\ &= e^{-\rho\sigma^2}\mathfrak{L}_{I_{intra}}(\rho)\mathfrak{L}_{I_{inter}}(\rho), \end{aligned} \quad (7)$$

where $\rho = \frac{\gamma_{th} r_0^\eta}{P_{q_0}\alpha}$, (a) was obtained using the exponential distribution of the channel g_{00}, and $\mathfrak{L}_{I_{intra}}(\cdot)$ and $\mathfrak{L}_{I_{inter}}(\cdot)$ are the Laplace transforms of I_{intra} and I_{inter}, respectively.

In order to derive the expression of the success probability, we need first to investigate the expressions of the Laplace transforms of I_{intra} and I_{inter}.

Theorem 1. *The Laplace transform of I_{intra} is given by:*

$$\mathfrak{L}_{I_{intra}}(\rho) \approx \prod_{q\in Q} \exp\Big(-2\pi a\lambda_{ED}\left(I_1(q) - I_2(q) - I_3(q)\right)\Big), \quad (8)$$

with $I_1(q) = \frac{\left(l_{q_0}+l_q\right)}{4T_c}\left(d_q^2 - d_{q-1}^2\right)$,

$$I_2(q) = \frac{min(l_q, l_{q_0})}{2T_c b(\eta+2)}\Big[d_q^2\Big(\eta b\,{}_2F_1\left(1, -\frac{2}{\eta}; \frac{\eta-2}{\eta}; -bd_q^{-\eta}\right) + 2d_q^\eta \log\left(bd_q^{-\eta}+1\right)\Big) - d_{q-1}^2\Big(\eta b\,{}_2F_1\left(1, -\frac{2}{\eta}; \frac{\eta-2}{\eta}; -bd_{q-1}^{-\eta}\right) + 2d_{q-1}^\eta \log\left(bd_{q-1}^{-\eta}+1\right)\Big)\Big], \quad (9)$$

$$I_3(q) = \frac{\left|l_{q_0}-l_{q_j}\right|}{2T_c b(\eta+2)}\Big[d_q^{\eta+2}\,{}_2F_1\left(1, \frac{\eta+2}{\eta}; \frac{\eta+2}{\eta}+1; -\frac{d_q^\eta}{b}\right) - d_{q-1}^{\eta+2}\,{}_2F_1\left(1, \frac{\eta+2}{\eta}; \frac{\eta+2}{\eta}+1; -\frac{d_{q-1}^\eta}{b}\right)\Big], \quad (10)$$

where ${}_2F_1(\cdot)$ is the Gaussian hypergeometric function [15], and $b = \frac{P_q}{P_{q_0}}\frac{min\left(l_q,l_{q_0}\right)}{l_{q_0}}\gamma_{th} r_0^\eta = \alpha P_q \frac{min\left(l_q,l_{q_0}\right)}{l_{q_0}}\rho$.

Proof. The proof is in Appendix C. □

Theorem 2. *The Laplace transform of I_{inter} is given by:*

$$\mathfrak{L}_{Inter}(\rho) \approx \prod_{q\in Q} exp\Big[-2\pi\lambda_G a N_q \frac{\pi}{\eta\sin(\pi\frac{2}{\eta})}\left(\alpha P_q\rho\right)^{\frac{2}{\eta}} \times \frac{1}{2Tc}\left(\frac{2\eta}{\eta+2} l_{q_0}\left(min(1, \frac{l_q}{l_{q_0}})\right)^{\frac{\eta+2}{\eta}} + \left(min(1, \frac{l_q}{l_{q_0}})\right)^{\frac{2}{\eta}} |l_{q_0} - l_q|\right)\Big]. \quad (11)$$

Proof. The proof is in Appendix D. □

Given (8) and (11), the general expression of P_{Succ} is given in (12).

$$P_{S\,uccc}(r_0,q_0)=e^{-\rho\sigma^2}\prod_{q\in Q}\left(e^{-2\pi a\lambda_{ED}(I_1(q)-I_2(q)-I_3(q))}e^{\frac{-2\pi^2\lambda_G aN_q}{\eta\sin(\pi\frac{2}{\hat{\eta}})}(\alpha P_q\rho)^{\frac{2}{\hat{\eta}}}\left(\frac{1}{2Tc}\frac{2\eta}{\eta+2}l_{q0}\left(min(1,\frac{l_q}{l_{q0}})\right)^{\frac{\eta+2}{\eta}}+\left(min(1,\frac{l_q}{l_{q0}})\right)^{\frac{2}{\hat{\eta}}}|l_{q0}-l_q|\right)}\right). \quad (12)$$

C. Special Cases

Here, we state few special cases deduced from our analytical results that can scale down to other published works:

(i) Perfect Orthogonality: If we consider perfect orthogonality, the transmission success probability simplifies to: $P_{S\,ucc}(r_0,q_0)=e^{-\rho\sigma^2}e^{-2\pi a\lambda_{ED}(I_1(q_0)-I_2(q_0))}e^{\frac{-2\pi^2\lambda_G aN_{q0}l_{q0}r_0^2\gamma_{th}^{\frac{2}{\hat{\eta}}}}{Tc(\eta+2)\sin(\pi\frac{2}{\hat{\eta}})}}$.

(ii) Single Gateway Toplogy: For a single gateway topology, only intra-cluster interference are considered: $P_{S\,ucc}(r_0,q_0)=e^{-\rho\sigma^2}\prod_{q\in Q}e^{(-2\pi a\lambda_{ED}(I_1(q)-I_2(q)-I_3(q)))}$.

(iii) Only one interfering SF: Considering the q'th SF: $P_{S\,ucc}(r_0,q_0)=e^{-\rho\sigma^2}e^{(-2\pi a\lambda_{ED}(I_1(q)-I_2(q)-I_3(q)))}\times e^{\frac{-2\pi^2\lambda_G aN_q}{\eta\sin(\pi\frac{2}{\hat{\eta}})}(\alpha P_q\rho)^{\frac{2}{\hat{\eta}}}\left(\frac{1}{2Tc}\frac{2\eta}{\eta+2}l_{q0}\left(min(1,\frac{l_q}{l_{q0}})\right)^{\frac{\eta+2}{\eta}}+\left(min(1,\frac{l_q}{l_{q0}})\right)^{\frac{2}{\hat{\eta}}}|l_{q0}-l_q|\right)}$.

(iv) Same Power Allocation: Assuming all the SFs use the same power, $P_q=P_{q0}$, and b in (8) simplifies to $\frac{min(l_q,l_{q0})}{l_{q0}}\gamma_{th}r_0^{\eta}$.

IV. Simulation Results

In this section, we validate our analytical model using Monte Carlo (MC) simulations. The packet size is fixed to 25 bytes. The packet time-on-air depends on the used SF and is calculated, based on each SF Data Rate [3] ($l_1=0.036$s, $l_2=0.064$s, $l_3=0.113$s, $l_4=0.204$s, $l_5=0.365$s, and $l_6=0.682$s). LoRa coverage radius for dense urban environment is 2 Km and a typical metropolitan area of 100 km^2 can be covered by 30 gateways [16]. Hence, in our simulation scenario we assumed R= 2km and λ_G(/Km^2)= 0.3. The bandwidth and the frequency are chosen according to LoRa regulations for the European region: Bw= 125 KHz and f$_c$ = 868 MHz , the contention window is $Tc=1.5$ Sec. Unless otherwise mentioned, the parameters used in the simulations are: $\eta=3$, a= 0.1, $\lambda_{ED}=100$ Nodes/Km^2 and $P_q=14$ dBm. To analyze the impact of power allocation on the performance, we tested two schemes: same power allocation and SF-based power allocation. For the first scheme, $P_q=14$ dBm $\forall$ q; while for the second, the power is attributed according to the used SF (Higher SFs are assigned higher powers) which is close to the way LoRa Adaptive Data Rate (ADR) works [17] ($P_1=2$ dBm, $P_2=5$ dBm, $P_3=8$ dBm, $P_4=11$ dBm, $P_5=14$ dBm, $P_6=20$ dBm). To calculate the performance metric, LoRa nodes are deployed according to a MCP and kept fixed for the simulation setup which is similar to real deployment scenarios in most smart city IoT applications. The desired node position is fixed based on the SF to investigate at $r_0(q)=d_{q-1}+\frac{\omega}{2}$ and its transmission status remains equal to 1 (always active). At each simulation step, the interfering nodes are determined based on their data status which follows

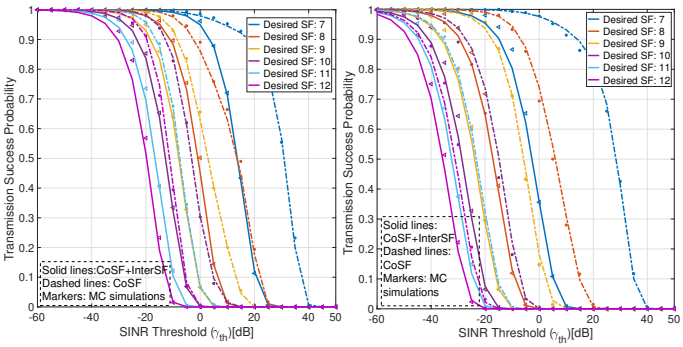

(a) Single Gateway topology (b) Multiple Gateway topology

Figure 2: Transmission success probability ($P_{S\,ucc}$) versus different SINR thresholds (γ_{th}).

a geometric distribution; once they have data to transmit, the transmission start time of each node is randomly generated following a uniform distribution. The collision overlap time with the desired packet is then calculated and multiplied by the interfering power. For MC simulations, the transmission success probability of each SF, under both perfect/imperfect SF orthogonality, is found by averaging over the number of simulations. In all the figures of this section, markers illustrate results obtained by MC simulation.

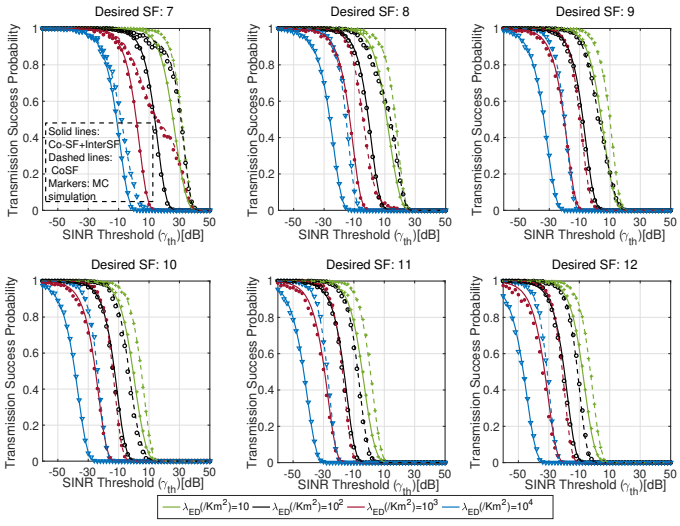

Figure 3: Transmission success probability versus SINR thresholds for different λ_{ED} in a single LoRa cell.

Fig.2 shows the transmission success probability of each desired SF versus different SINR thresholds for both single gateway topology and multi-gateway topology. Solid lines illustrate the impact of both interference types (Co-SF and

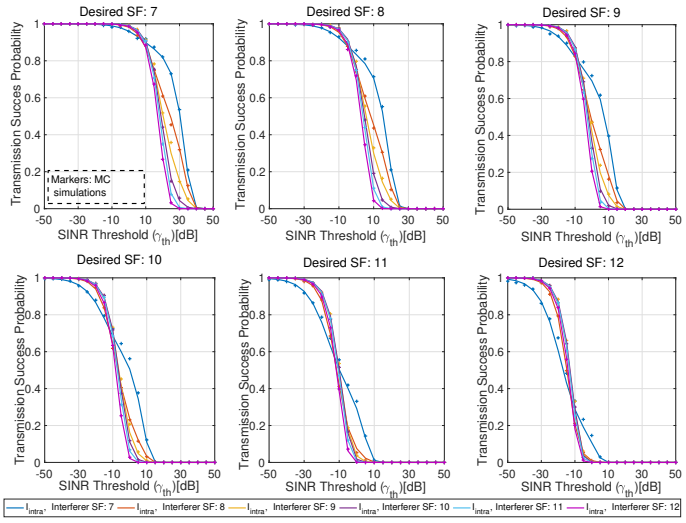

Figure 4: Transmission success probability versus SINR thresholds under Per-SF interference and same power allocation in a single LoRa cell with $\lambda_{ED} = 200$ Nodes/Km^2.

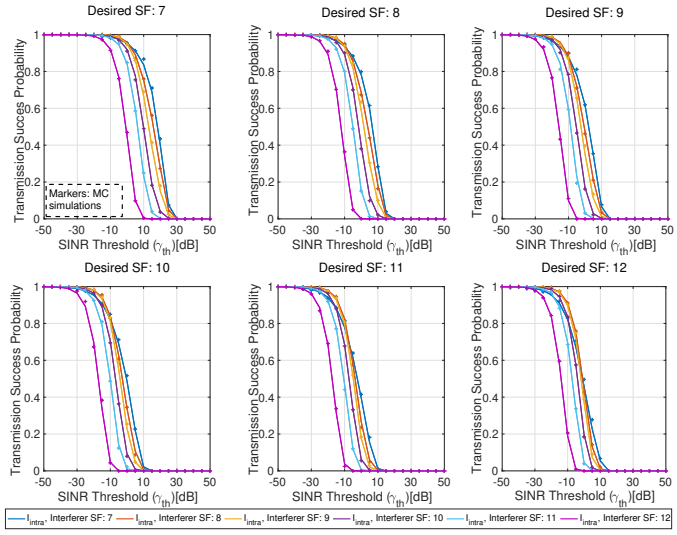

Figure 5: Transmission success probability versus SINR thresholds under Per-SF interference and SF-based power allocation in a single LoRa cell with $\lambda_{ED} = 200$ Nodes/Km^2.

Inter-SF), while dashed lines illustrate the impact of only Co-SF interference. We can see that for each SF the probability of successful transmission under aggregated interference from different SFs is considerably lower than the result obtained by considering only Co-SF interference. Hence, we can say that the perfect orthogonality assumption commonly used results in an overestimation of the network performance which may impact the network dimensioning and planning. We can see also that, as expected, packet transmission success decreases when SF increases. This can be explained by the fact that higher SFs have longer time on air which leads to longer time overlap with the desired packet and hence higher interference exposure.

In Fig.3, we plotted the transmission success probability of different desired SFs under both aggregated interference and only co-SF interference, for different devices densities in a LoRa gateway. Higher nodes densities degrade all the SFs performance and its impact is much important for higher SFs as it appears for SF= 11 and SF= 12.

To assess the impact of SFs on one another performance, we plotted in Fig.4 and Fig.5 the transmission success probability of each SF under interference from one specific interfering SF-set. In Fig.4, we considered the same power allocated to all the nodes independently from the used SF; while in Fig.5, we used the SF-based power allocation scheme which is closer to the way LoRa ADR works. An examination of these figures reveals that for the case of same power allocation, at lower SINR thresholds, lower SFs tend to have the worst impact on the success probability while at higher SINR thresholds, higher SFs have the worst impact. This observation stresses the importance of SF allocation on the network performance. Under SF-based power allocation, only one common behaviour for all the SFs is recognized: higher SFs decrease transmission success probability more, independently of the SINR threshold. This observation is more aligned with the commonly believed fact that the higher SFs induce more interference as they stay active for longer in the network. Moreover, the SF-based power allocation decreases the performance of lower SFs and improves the performance of higher SFs, compared to the same power allocation. This shows that the preference of same or SF-based power allocation scheme depends on the SF of the desired node. For instance, in the case of desired SF= 12, for an SINR threshold equal to -10dB, the success probability is around 30% for all interfering SFs, whereas under the SF-based power allocation the success probability overcomes 70% for SFs lower than 11.

Figs.4, 5 and 3 confirm that decoding thresholds are not fixed and do not depend only on the SF of desired and interfering nodes, they are also impacted by the nodes density and the power allocation. These thresholds decrease when the interfering SF increase and when the nodes density becomes higher.

V. Conclusion

Using stochastic geometry, we analysed the transmission success probability of a multi-gateway LoRa-based LPWA network. We demonstrated that limiting the analysis to the impact of Co-SF interference specifically can lead to an over-estimation of the network performance. The incorporation of time dimension with the formulated collision overlap function better depicts the interference temporal dynamic and makes, as a result, the analysis more realistic. We also showed that power allocation schemes play a significant role in the vulnerability of each SF to interference and that decoding thresholds depend on several network parameters. Uniquely, our results suggest that activating an adaptive power allocation schemes like LoRa ADR would be advantageous for nodes far from the gateway more than other nodes. This observation suggests a potential future work to validate this behaviour in a real deployment scenario.

References

[1] U. Noreen, L. Clavier, and A. Bounceur, "LoRa-like CSS-based PHY layer, Capture effect and serial interference cancellation," in *European Wireless 2018; 24th European Wireless Conference*, 2018, pp. 1–6.

[2] Z. Qin, Y. Liu, G. Y. Li, and J. A. McCann, "Modelling and analysis of low-power wide-area networks," in *IEEE International Conference on Communications (ICC'2017)*, May 2017, pp. 1–7.

[3] O. Georgiou and U. Raza, "Low power wide area network analysis: Can LoRa scale?" *IEEE Wireless Communications Letters*, vol. 6, no. 2, pp. 162–165, April 2017.

[4] D. Croce, M. Gucciardo, S. Mangione, G. Santaromita, and I. Tinnirello, "Impact of LoRa imperfect orthogonality: Analysis of link-level performance," *IEEE Communications Letters*, vol. 22, no. 4, pp. 796–799, April 2018.

[5] A. Waret, M. Kaneko, A. Guitton, and N. El Rachkidy, "LoRa throughput analysis with imperfect spreading factor orthogonality," *IEEE Wireless Communications Letters*, vol. 8, no. 2, pp. 408–411, April 2019.

[6] C. Caillouet, M. Heusse, and F. Rousseau, "Optimal SF Allocation in LoRaWAN Considering Physical Capture and Imperfect Orthogonality," in *GLOBECOM 2019 - IEEE Global Communications Conference*, Waikoloa, United States, Dec. 2019.

[7] L. Beltramelli, A. Mahmood, M. Gidlund, P. Österberg, and U. Jennehag, "Interference modelling in a multi-cell LoRa system," in *14th International Conference on Wireless and Mobile Computing, Networking and Communications (WiMob'2018)*, October 2018, pp. 1–8.

[8] J. Lim and Y. Han, "Spreading factor allocation for massive connectivity in LoRa systems," *IEEE Communications Letters*, vol. 22, no. 4, pp. 800–803, April 2018.

[9] B. Błaszczyszyn and P. Mühlethaler, "Analyzing lora long-range, low-power, wide-area networks using stochastic geometry," in *Proceedings of the 12th EAI International Conference on Performance Evaluation Methodologies and Tools*. New York, NY, USA: Association for Computing Machinery, 2019, p. 119–126.

[10] C. Goursaud and J.-M. Gorce, "Dedicated networks for IoT : PHY / MAC state of the art and challenges," *EAI Endorsed Transactions on Internet of Things*.

[11] F. Benkhelifa, Z. Qin, and J. McCann, "Minimum throughput maximization in lora networks powered by ambient energy harvesting," in *ICC 2019 - 2019 IEEE International Conference on Communications (ICC)*, 2019, pp. 1–7.

[12] H. ElSawy, A. Sultan-Salem, M. Alouini, and M. Z. Win, "Modeling and analysis of cellular networks using stochastic geometry: A tutorial," *IEEE Communications Surveys Tutorials*, vol. 19, no. 1, pp. 167–203, 2017.

[13] B. Błaszczyszyn and P. Mühlethaler, "Interference and SINR coverage in spatial non-slotted Aloha networks," *Anals of Telecommunications*, vol. 70, no. 7, pp. 345–358, August 2015.

[14] M. Haenggi, *Stochastic Geometry for Wireless Networks*. Cambridge University Press, 2012.

[15] Alan Jeffrey, Daniel Zwillinger, I. Gradshteyn, and I. Ryzhik, Eds., *"Table of Integrals, Series, and Products (Seventh Edition)"*, seventh edition ed. Boston: Academic Press, 2007, pp. 1063 – 1068.

[16] M. O. Farooq and D. Pesch, "Analyzing LoRa: A Use Case Perspective," in *2018 IEEE 4th World Forum on Internet of Things (WF-IoT)*, 2018, pp. 355–360.

[17] N.Sornin(Semtech), M.Luis(Semtech), T.Eirich(IBM), T. Kramp (IBM), and O.Hersent(Actility), "LoRaWAN™ Specification," 2015.

[18] J.Tang, G.Chen, J.Coon, and D.E.Simmons, "Distance distributions for Matèrn cluster processes with application to network performance analysis," *IEEE ICC*, 2017.

Appendix A
Proof of Lemma 1

Assuming an interfering node located at x_{ij} that starts transmitting its packet of duration l_q at instant T_{ij} randomly in a contention window $[-T_c, T_c]$. Then, the collision time overlap between x_j and the typical user is given by:

- If $l_q \leq l_{q_0}$,

$$h_{q_0,q}(T_{ij}) = \begin{cases} \frac{l_{q_0}-T_{ij}}{l_{q_0}}, & \text{if } l_{q_0}-l_q \leq T_{ij} \leq l_{q_0}, \\ \frac{l_q}{l_{q_0}}, & \text{if } 0 \leq T_{ij} \leq l_{q_0}-l_q, \\ \frac{l_q+T_{ij}}{l_{q_0}}, & \text{if } -l_q \leq T_{ij} \leq 0, \\ 0 & \text{if} -T_c \leq T_{ij} < -l_q \quad \text{or} \quad l_{q_0} < T_{ij} \leq T_c. \end{cases}$$

- If $l_q > l_{q_0}$,

$$h_{q_0,q}(T_{ij}) = \begin{cases} \frac{l_{q_0}-T_{ij}}{l_{q_0}}, & \text{if } 0 \leq T_{ij} \leq l_{q_0}, \\ 1, & \text{if } l_{q_0}-l_q \leq T_{ij} \leq 0, \\ \frac{l_q+T_{ij}}{l_{q_0}}, & \text{if } -l_q \leq T_{ij} \leq l_{q_0}-l_q, \\ 0 & \text{if} \quad -T_c \leq T_{ij} < -l_q \quad \text{or} \quad l_{q_0} < T_{ij} \leq T_c. \end{cases}$$

Appendix B
Proof of Corollary 1

Assuming that the transmission start time of LoRa active nodes follows a uniform distribution $T_{ij} \overset{Dist}{=} U(-T_c, T_c)$ and using Lemma 1, we evaluate $\mathbb{E}_{T_{ij}}\left[\frac{1}{1+sh_{q_0,q}(T_{ij})}\right]$ for $l_q \leq l_{q_0}$ as

$$\begin{aligned} \mathbb{E}_t\left[\frac{1}{1+uh_{q_0,q}(T_{ij})}\right] &= \frac{1}{2T_c}\Bigg[\int_{-T_c}^{-l_q} dt + \int_{-l_q}^{0} \frac{1}{1+u\frac{t+l_q}{l_{q_0}}}dt \\ &+ \int_{0}^{l_{q_0}-l_q} \frac{1}{1+u\frac{l_q}{l_{q_0}}}dt + \int_{l_{q_0}-l_q}^{l_{q_0}} \frac{1}{1+u\frac{l_{q_0}-t}{l_{q_0}}}dt + \int_{l_{q_0}}^{T_c} dt\Bigg] \\ &= 1 - \frac{l_{q_0}+l_q}{2T_c} + \frac{l_{q_0}}{T_c u}\log\left(\frac{ul_q}{l_{q_0}}+1\right) + \frac{l_{q_0}-l_q}{2T_c\left(1+u\frac{l_q}{l_{q_0}}\right)}. \end{aligned} \tag{13}$$

Similarly, we show for $l_q > l_{q_0}$, that

$$\mathbb{E}_t\left[\frac{1}{1+uh_{q_0,q}(T_{ij})}\right] = 1 - \frac{l_{q_0}+l_q}{2T_c} + \frac{l_{q_0}\log(u+1)}{T_c u} - \frac{l_{q_0}-l_q}{2T_c(1+u)}. \tag{14}$$

Appendix C
Proof of Theorem 1

$$\mathfrak{L}_{I_{intra}}\{s\} = \mathbb{E}_{x,G,t}\left[e^{-s\sum_{q\in Q}\sum_{x_j\in\tilde{\Phi}_{ED,0,q}\setminus x_0} P_q h_{q_0,q}(T_{ij})\alpha\|x_{0,j}\|^{-\eta} g_{0j}}\right] \tag{15}$$

$$\begin{aligned} &= \mathbb{E}_{x,G,t}\left[\prod_{q\in Q}\prod_{x_j\in\tilde{\Phi}_{ED,0,q}\setminus x_0} e^{-sP_q h_{q_0,q}(T_{ij})\alpha\|x_{0,j}\|^{-\eta} g_{0j}}\right] \\ &\overset{(a)}{=} \mathbb{E}_{x,t}\left[\prod_{q\in Q}\prod_{x_j\in\tilde{\Phi}_{ED,0,q}\setminus x_0} \frac{1}{1+sP_q h_{q_0,q}(T_{ij})\alpha\|x_{0,j}\|^{-\eta}}\right] \\ &\overset{(b)}{\approx} \prod_{q\in Q}\left[\mathbb{E}_{x,t}\prod_{x_j\in\tilde{\Phi}_{ED,0,q}\setminus x_0} \frac{1}{1+sP_q h_{q_0,q}(T_{ij})\alpha\|x_{0,j}\|^{-\eta}}\right] \\ &\overset{(c)}{=} \prod_{q\in Q}\left[e^{-2\pi a\lambda_{ED}\int_{d_{q-1}}^{d_q}\left(1-\mathbb{E}_t\left[\frac{1}{1+sP_q h_{q_0,q}(T_{ij})\alpha r^{-\eta}}\right]\right)rdr}\right], \end{aligned}$$

where (a) is explained by the independence of channel gains from both the spatial and temporal dimensions and is obtained using the moment generating function (MGF) of the exponential distribution with mean 1, (b) is an approximation obtained

using Fortuin–Kasteleyn–Ginibre (FKG) inequality for $T_{ij} > 0$ and extended to $\forall\ T_{ij}$ through validation by MC simulations, and (c) is obtained by applying the probability generating function (PGFL) of $\tilde{\Phi}_{ED,i}$ and the change of integration coordinates from Cartesian to polar. Using Corollary 1, we obtain (8).

Appendix D
Proof of Theorem 2

$$\begin{aligned}
&\mathfrak{Q}_{I_{inter}}\{s\} \qquad (16)\\
&\overset{(a)}{=} \mathbb{E}_{y,x,t}\left[\prod_{q\in Q}\prod_{y_i\in\Phi_G}\prod_{x_j\in\tilde{\Phi}_{ED,i,q}}\frac{1}{1+sP_q h_{q_0,q}(T_{ij})\alpha\|y_i+x_{ij}\|^{-\eta}}\right]\\
&\overset{(b)}{\approx} \prod_{q\in Q}\mathbb{E}_{y,x,t}\left[\prod_{y_i\in\Phi_G\setminus y_0}\prod_{x_j\in\tilde{\Phi}_{ED,i,q}}\frac{1}{1+sP_q h_{q_0,q}(T_{ij})\alpha\|y_i+x_{ij}\|^{-\eta}}\right]\\
&\overset{(c)}{=} \prod_{q\in Q} exp\left(-2\pi\lambda_G\int_0^{\infty}(1-\xi_q(s,y))ydy\right),
\end{aligned}$$

Following similar steps to $\mathfrak{Q}_{I_{intra}}$, (a) is obtained using the independence of channel gains from both the spatial and temporal dimensions and the MGF of the exponential distribution, (b) is an approximation obtained using FKG inequality for $T_{ij} > 0$ and extended to $\forall\ T_{ij}$ through validation by MC simulations, and (c) is obtained using the PGFL of the Matern cluster process [18] with

$$\xi_q(s,y) = e^{-\lambda_{ED}a\int_{d_{q-1}}^{d_q}\int_0^{2\pi}\left(1-E_t\left(\frac{1}{1+sP_q h_{q_0,q}(T_{ij})\alpha\beta(x,y,\theta)^{-\eta}}\right)\right)xdxd\theta}, \quad (17)$$

with $\beta(x,y,\theta) = \sqrt{y^2+x^2-2xycos(\theta)}$. For the case of a highly clustered network we have $x << y$. Using the approximation in Corollary 2 [2], we have $\beta(x,y,\theta) \approx y$ and doing a Taylor series expansion we obtain:

$$\begin{aligned}
\mathfrak{Q}_{I_{inter}}\{s\} &= \prod_{q\in Q} e^{-2\pi\lambda_G\lambda_{ED}aN_q)\int_0^{\infty}\int_{-\infty}^{+\infty}\left(\frac{sP_q h_{q_0,q}(t)\alpha y^{-\eta}}{1+sP_q h_{q_0,q}(t)\alpha y^{-\eta}}\right)f_{T_{ij}(t)}ydtdy}\\
&\overset{(d)}{=} \prod_{q\in Q} e^{-2\pi\lambda_G\lambda_{ED}aN_q\frac{\pi(sP_q\alpha)^{\frac{2}{\eta}}}{\eta\sin(\pi\frac{2}{\eta})}\int_{-\infty}^{+\infty}(h_{q_0,q}(t))^{\frac{2}{\eta}}f_{T_{ij}(t)}dt},
\end{aligned}$$

where (d) is obtained using [15, (3.241)]. Recalling Lemma 1, we evaluate $\int_{-\infty}^{+\infty}(h_{q_0,q}(t))^{\frac{2}{\eta}}f_{T_{ij}(t)}dt$. For $s = \rho$, we obtain the final expression in (11).